William Singhose
Professor
Georgia Institute of Technology
Woodruff School of Mechanical Engineering
USA

Kelvin Peng
Graduate Research Assistant
Georgia Institute of Technology
Woodruff School of Mechanical Engineering
USA

Anthony Garcia
Graduate Research Assistant
Georgia Institute of Technology
Woodruff School of Mechanical Engineering
USA

Aldo Ferri
Professor
Georgia Institute of Technology
Woodruff School of Mechanical Engineering
USA

Modeling and Control of Crane Payload Lift-off and Lay-down Operations

When crane payloads are lifted off the ground, the payload may unexpectedly swing sideways. This occurs when the payload is not directly beneath the hoist. Because the hoist point is far above the payload, it is difficult for crane operators to know if the hoist cable is perfectly vertical before they start to lift the payload. Some amount of horizontal motion of the payload will always occur at lift off. If an off-centered lift results in significant horizontal motion, then it creates a hazard for the human operators, the payload, and the surrounding environment. This paper presents dynamic models of off-centered lifts and experimental verification of the theoretical predictions. The inverse problem of setting a large payload on the ground can also be challenging. For example, when laying down a long payload starting from a near-vertical orientation in the air, to a horizontal position on a flat surface, the payload can unexpectedly slide sideways. This paper presents motion-control solutions that aid operators performing challenging lay-down operations.

Keywords: *cranes, payload swing, crane safety.*

1. INTRODUCTION

Cranes are ubiquitous machines that provide essential heavy lifting capabilities for a wide range of industries. Although cranes are very useful, and are one of the most successful machines in the history of engineering, they are also dangerous machines that have several failure modes. One of the most common causes of crane-related injuries and fatalities is "side pull"[1], wherein the payload hoist cable does not hang straight down, but rather to the side. In such cases, dangerous payload sliding and swinging may occur.

In a typical lift, the hook is suspended from the trolley by hoist cable(s) and attached to the payload with an arrangement of rigging cable(s). The correct procedure for lifting is to position the hoist directly over the payload's center of mass[2]. However, accurately positioning the overhead trolley may be challenging for the crane operator because the position of the hoist is difficult to judge, especially when it is high above the payload.

An off-centered lift occurs when the payload is horizontally offset from the hoist. This situation is shown in Figure 1. If the crane hoists in this configuration, then the payload may slide sideways, and swing in the air when it comes off the ground. Clearly, this presents an undesirable dynamic effect.

Most crane-related research publications focus on modeling a payload swinging in the air while payload interaction with the ground is largely ignored. The most popular choice to model the swinging payload is the lumped-mass single pendulum [3]. Some prior work used more complex models to address specific situations such as varying the hoist cable length [4, 5], double pendulums [6-8], and distributed loads [9].

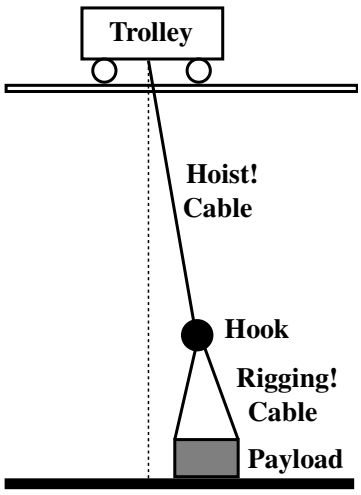

Figure 1: Off-centre crane payload hoist

Barrett and Hrudey investigated lifting payloads off the ground using various hoist cable tensions[10]. However, their work focused on the dynamic forces exerted on the crane structure, rather than the motion of the payload. Modeling the contact dynamics and friction between the payload and ground is a crucial part of understanding the dynamics of off-centered lifts. A number of contact modes can exist between the payload and ground: stiction (zero relative tangential velocity between contact surfaces), sliding/slipping (non-zero relative velocity), and separation of contact (non-zero normal velocity) [11]. The choice of friction model is important for determining the mode of contact.

In order to limit dangerous effects of off-center lifts, a control system can be added to the crane that aids the human operator by automatically centering the trolley over the payload. A commercial product containing such

Received: September 2015, Accepted: April 2016
Correspondence to: William Singhose
Georgia Insitute of Technology, Woodruff School of Mechanical Engineering, USA
E-mail: william.singhose@me.gatech.edu
doi:10.5937/fmet1603237S

a semi-automatic trolley positioning system has recently been installed at several automobile manufacturing plants [12, 13]. A block diagram illustrating such a control system is shown in Figure 2.The commercial product is based entirely on feedback control and does not utilize knowledge of payload sliding and swinging dynamics.

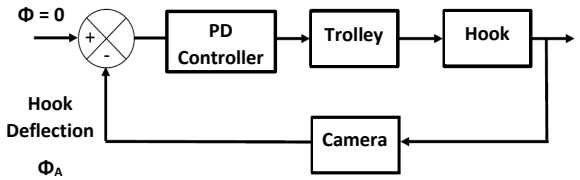

Figure 2: Control Block Diagram.

This paper develops dynamic sliding and contact modeling approaches that can be used to improve lift-off control. A two-dimensional model is presented here; however, it can be extended to 3D[14]. This model is used to efficiently produce simulation responses, from which, situations that lead to dangerous levels of sliding and swinging can be identified. The fidelity of the model is verified with experimental results from a 10-ton bridge crane.

The inverse problem of setting a large payload on the ground can also be challenging. For example, when laying down a long payload starting from a near-vertical orientation in the air, to a horizontal position on a flat surface, the payload can unexpectedly slide sideways. This paper also presents motion-control solutions that aid operators to perform challenging lay-down tasks

2. MODELING OF LIFT-OFF DYNAMICS

A two-dimensional model developed previously [15] was able to capture the aggregate behavior of the payload and was used to perform an analysis of the controller now implemented at several automobile plants including those of General Motors, Toyota, and Hyundai [13]. However, to further improve auto-centering control methods for off-centered crane lifts, such as dealing with more complex payload shapes, our understanding of the dynamic effects must be improved. Areas that limit our understanding include: accurate sliding dynamics, dynamics of impacts, the need to enumerate different contact modes that each consist of several motion equations, and the transition laws between modes.

The main limitation of previous models is the representation of the ground and payload interaction and the need to switch between multiple models. Ideally, the dynamics of the system would be captured with a single set of governing equations, while accurately capturing sliding and impact behaviors.

2.1 Payload-Ground Interaction Model

Modeling the interaction between the payload and ground is crucial for understanding off-centered lifts. Therefore, the contact dynamics and friction modeling are very important. There are a number of velocity-dependent contact modes that can exist between the payload and the ground: friction, sliding/slipping, and separation of contact [11]. The choice of friction model is important for determining the mode of contact.

Perhaps the most often-used friction model is the Coulomb model [15]:

$$\begin{aligned} f_f &\leq \mu_s \quad |f_N| : \text{friction} \\ f_f &= \mu_k \quad |f_N| : \text{sliding} \end{aligned} \tag{1}$$

where f_f and f_N are the tangential friction and normal forces, respectively; and μ_s and μ_k are the static and kinetic coefficients of friction, respectively. This model is commonly used because of its simplicity and ability to capture important dynamic effects. As it can be seen in (1), the friction force is composed of two distinctly defined velocity states. In instances where the velocity is zero (stiction), the entity needs to experience a force greater than the normal force multiplied by a static friction coefficient to start moving. When in motion (sliding), the magnitude of friction force is the normal force multiplied by the kinetic friction coefficient, in the direction opposing the motion.

The discontinuous behavior representing the slip-stick transition is difficult to simulate. To address this problem, a number of researchers have used a "regularized" friction law; see for example [15]. By defining a very steep linear relationship, with a slope of μ_s/ε where ε is an appropriately small number, modeling the friction force can be done with a continuous transition definition for velocities around zero which defines the slip-stick region. This eliminates the discontinuity in representing the friction states.

A velocity-based function for the kinetic friction coefficient is also used in the Stribeck model [16] to capture more accurate sliding dynamics. The function of the envelope transitioning from the static coefficient to the kinetic coefficient is described by a decaying exponential function of the velocity in the form $e^{(-|v|/v_m)}$, where v_m is a defined parameter.

Applying these concepts to the friction model simplifies the simulation, while improving accuracy, yielding behavior demonstrated in Figure 3.

The contact dynamics between the payload and the ground could be modeled using either continuous-compliant models or discrete models. In an earlier model [15], a discrete approach was taken, by simply solving a mechanics problem of different enumerated contact "modes". One issue encountered was the static indeterminacy due to multiple ground contact points of the payload.

This was avoided by solving a moment-couple, in addition to Mason's approach [11] of enumerating the contact modes, solving and checking. The problem of multiple contacts has been addressed by [17] using a Linear Complementarity Problem (LCP) approach to solving for friction forces and accelerations. Such an approach would eliminate difficulties arising from the enumerated process, however LCP itself is a relatively cumbersome and computationally intensive method.

Another way to avoid the circularity issue of accelerations and forces for multiple contact points is to use a continuous-compliant reaction force approach[18].

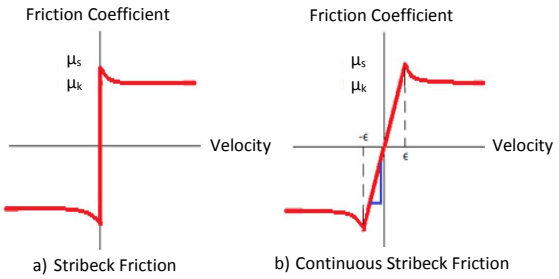

Friction 3: Friction Model.

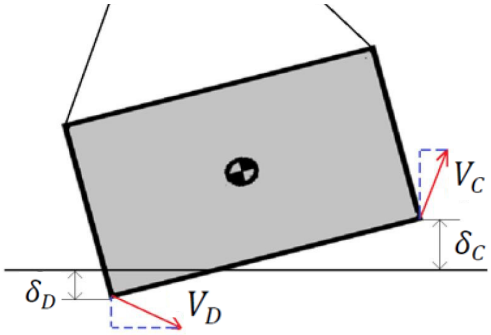

Figure 4: Payload-Ground Interaction Model.

This involves determining forces solely as functions of displacements and velocities.

The methodology of determining the force based on displacements and velocity can be done by representing contacts as a form of a spring-damper system. This approach, in its simplest form, is known as the Kelvin-Voigt model. Here the contact normal force is simply defined as:

$$F_N = C_d\dot{\delta} + K_s\delta \tag{2}$$

where C_d and K_s are the damping and spring coefficients, respectively. The value δ is a measurement of local indentation, even though realistically a penetration of the objects may not be possible. Such an approach is permissible if the indentation is kept at a negligible value compared to the system dynamic motions. A representation of the displacement and velocity of the contact points is shown in Figure 4.

In the contact modeling survey done by Gilardi[18], it is mentioned that one of the main weaknesses of this approach is that the damping term acts to hold the objects together as they are separating. To overcome this issue, a "one-way" compressive damper was implemented [19].

This approach yields the following representation of the reaction normal compliant forces:

$$F_{NKi} = \begin{cases} 0 & \delta_t > 0, \\ -K_s\delta_i & \delta_t \le 0. \end{cases} \tag{3}$$

$$F_{NCi} = \begin{cases} C_d\dot{\delta}_i & \delta_i \le 0, \dot{\delta}_i \le 0 \\ 0, & \text{else} \end{cases} \tag{4}$$

$$F_{Nt} = F_{NCt} + F_{NKi} \tag{5}$$

where i=C and D. C is the bottom right corner and D is the bottom left corner of the rectangular payload, as shown in Figure 4.

2.2 Crane Lifting Component Models

The payload lifting system consists of two different sets of cables, the rigging that attaches the hook to the payload, and the hoist cable that raises the hook. The hoist cable can be reasonably modeled as a massless stiff rod because the hook mass is usually sufficient to keep the cables in tension throughout the lift[15].

As for rigging cables, this same assumption cannot be made because there are instances where these cables are slack. Therefore, massless springs are used to represent the tension forces of the cables. This model only exerts forces by the cables when the riggings are taut. If the rigging cables are shorter than their original lengths, then they are assumed to be slack and no forces are generated.

However, in cases of impact, the transition from tension to slack occurs frequently and results in significant energy losses. These losses were not captured by the earlier model [15]. Therefore, application of a damping term is introduced as a means to accurately capture the dissipating energy, similar to earlier methods [20].

When considering double-pendulum dynamics, a means to capture energy losses during the swinging motion is achieved by applying light damping to the trolley ($M_{Trolley}$) and hook (M_{Hook}) pivots. In both cases, a torsional spring and torsional damper are applied.

3. TWO-DIMENSIONAL MODEL

To verify that the modeling approaches for the ground-payload interaction and other crane lifting component forces described above are valid for simulating off-centered crane lifts, a two-dimensional dynamic model of the complete system was developed and experimentally verified.

3.1 Two-Dimensional Dynamic Model

Figure 5 shows the main elements of the two-dimensional model. Note that the damping of the hook is actually a phantom damper, as the moments about the hook are never actually calculated. This is done by applying a force at the payload center of mass using the relationship τ=Fr. The displacement and their rates are determined from the position and velocities of the hook and payload center of mass. By implementing these extra damping modifications along with the friction and contact dynamic models, an accurate and robust dynamic model is obtained as:

$$m_p a_x = F_{fC} + F_{fD} + T_{1x} + T_{2x} + F_{MHookx} \tag{6a}$$

$$m_p a_y = F_{NC} + F_{ND} + T_{1y} + T_{2y} + F_{MHooky} \tag{6b}$$

$$I_p\ddot{\alpha}\,\vec{k} = (\vec{r}_C \times \vec{F}_C) + (\vec{r}_D \times \vec{F}_D) + \\ +(\vec{r}_{T_1} \times \vec{T}_1) + (\vec{r}_{T_2} \times \vec{T}_2) \tag{6c}$$

$$I_h\ddot{\varphi} + m_h Lg\sin\varphi + 2m_h L\dot{L}\dot{\varphi} = \\ = M_{Trolley} + M_{T1} + M_{T2} \tag{6d}$$

where a_x, a_y, α, and ϕ are the acceleration in the horizontal direction of the center of mass, acceleration in the vertical direction of the center of mass, the angle of the payload with respect to the ground, and the angle of the hoist cable respectively. The length of the hoist cable is assumed to be retracted at the constant rate of $\dot{L} = -v$ which is relatively slow compared to the rest of the system dynamics. M_{T1} and M_{T2} are the moments about the trolley pivotcaused by the rigging cables. Finally, the corner forces in (6c) can be written in terms of their friction and normal components:

$$\vec{F}_C = F_{fC}\,\vec{i} + F_{NC}\,\vec{j}; \quad \vec{F}_D = F_{fD}\,\vec{i} + F_{ND}\,\vec{j} \qquad (7)$$

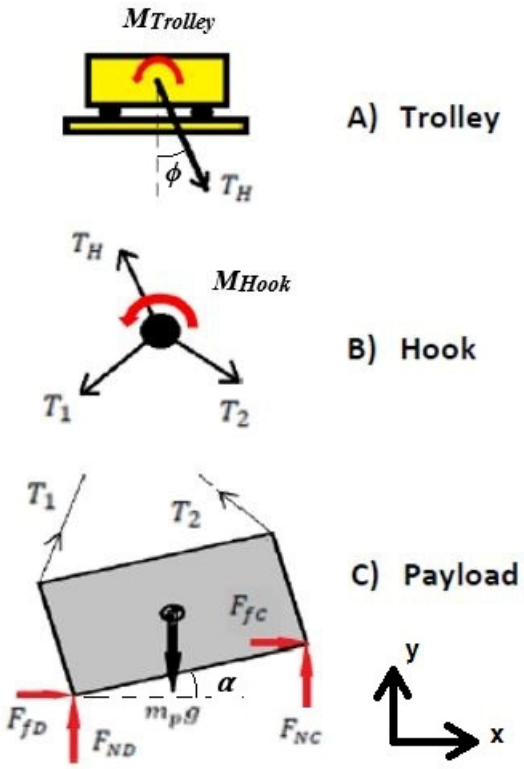

Figure 5: Main Elements of the Crane Model.

3.2 Two-Dimensional Experimental Set-up

The two-dimensional model was verified using experimental results from a gantry crane at the Georgia Institute of Technology Advanced Cranes Laboratory. The experimental setup is shown in Figure 6. The crane has sensing devices that accurately track the positions of the trolley and hook.

Tracking of the position of the payload corners was achieved by processing images taken by a high definition camera. To easily locate the corners of the payload, colored tape was used to cover the edges. By filtering out the colored tape from the sequence of images, the payload edges were clearly defined.

Even with the vision system implemented, it was still difficult to accurately determine when the payload actually made contact with the ground. To detect instances of contact, an NI myRIO embedded hardware device operating binary contact sensors was placed on-board the payload. The individual contact sensors were attached to the payload corners, collecting data in real time every 10ms.

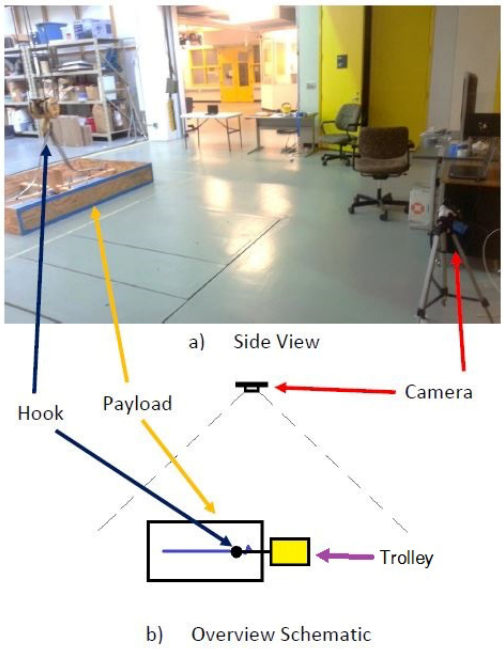

Figure 6: Experimental Set-Up.

3.3 Two-Dimensional Model Validation

The variables that were utilized in the simulation are listed in Table 1. Each of these parameters were tuned by separate experiments whenever possible, prior to simulating an off-centered crane lift where all the variables would be interrelated.

Table 1: Model Parameters.

K_{ground}	100000 N/m
C_{ground}	45000 Ns/m
K_{rig}	1132100 N/m
C_{rig}	11321 Ns/m
K_{hook}	0 N/rad
C_{hook}	0 Ns/rad
K_{pulley}	60 N/rad
C_{pulley}	60 Ns/rad
μ_k	0.169
μ_s	0.316
v_m	0.9 m/s

The friction coefficients were determined experimentally by using the crane to drag the payload along the ground. With knowledge of the payload mass, the hook mass, hoist cable angle and hoist cable length, the friction coefficients could be determined. The static friction coefficient was found by taking the sum of forces, while the kinetic coefficient was determined using work-energy relationships. The parameter υ_m, was tuned manually based on sliding behavior observed and recorded from experiments.

The contact model parameters were determined based on a desired tolerance of the payload penetration through the ground. The spring and damping coefficients for the ground were set so that the payload would not exceed a 2mm penetration of the ground when at rest. In setting these values, a convergence

study of the reaction compliant forces was performed indicating that the system dynamics are not sensitive to variations of the spring and damping parameters. Therefore, as long as the desired tolerance on the maximum penetration is satisfied, these values can be adjusted to achieve the best representation of impacts.

For the rigging parameters, an experiment was performed to determine how much damping should be utilized in the model. The test involved lifting the hanging payload up 10cm and dropping it slightly without ground contact, to observe the response of the rigging cables in cases of changing from a state of slack to tension. It was observed that the payload reached a rest position almost instantaneously. Simulating this situation with springs alone caused the payload to experience an unrealistic bouncing effect when the rigging cables transitioned from slack to tension. By implementing damping components in the rigging cables, a more accurate representation was achieved.

Lastly, the lightly-damped torsion damping of the pulley and hook were tuned based on measurements of the oscillations of the pendulum swinging motions.

In order to verify the parameter tuning, off-centered lifting experiments with friction, sliding, swinging and impact were performed. Prior to comparing the experimental results with the model, the case of an off-centered crane lift consisting of a 1.2m horizontal offset and lifted to 5cm above the ground, forcing impact cases during the swinging motion, was simulated using an earlier model[15].

As shown in Figure 7 unstable dynamic behavior appears over an extended period of time, involving impact situations. The unstable behavior arises from a combination of different aspects of the model, ranging from the difficulties in defining the transitions between enumerated contact modes to the lack of damping present in the system representation. Utilizing the model described in this section, instability issues have been eliminated.

Figure 8 compares experimental and simulation results using the model of the payload's bottom corner positions in the horizontal (x) direction. It can be seen that the simulation accurately captures both the sliding behavior during the first 12 seconds, and the oscillatory swinging motions after complete lift-off.

As for the bottom corner positions in the vertical (y) direction, simulation results are shown in Figure 9a and the corresponding experiment results in Figure 9b. It can be seen in Figure 9a that the corner positions oscillate in an alternating manner with several cases of contact with the ground. Comparing these results with Figure 9b, the general oscillation behavior matches. Most importantly, the number of repeated contacts on the same corner occurs in both the simulation and the experimental results up to 25 seconds, as shown in Figure 10.

As we can see in the results presented above, there is significant improvement over the earlier model. The implementation of the ground and payload interaction model eliminated the presence of negative normal forces in cases of impacts, which arose in the original model due to the difficulty of defining appropriate transition laws between contact modes. Furthermore, the application of damping allowed the simulation to capture a more accurate dynamic representation of the complete system, including cases of impact.

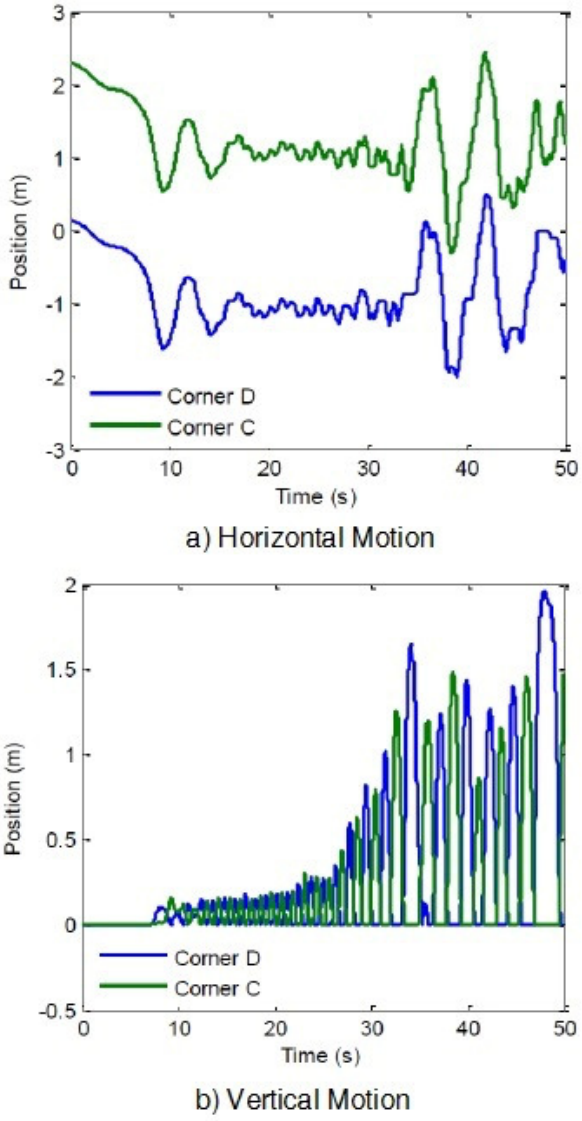

Figure 7: Bottom Corner Positions Predicted by Earlier Model (lift height 5cm, initial offset 1.2m).

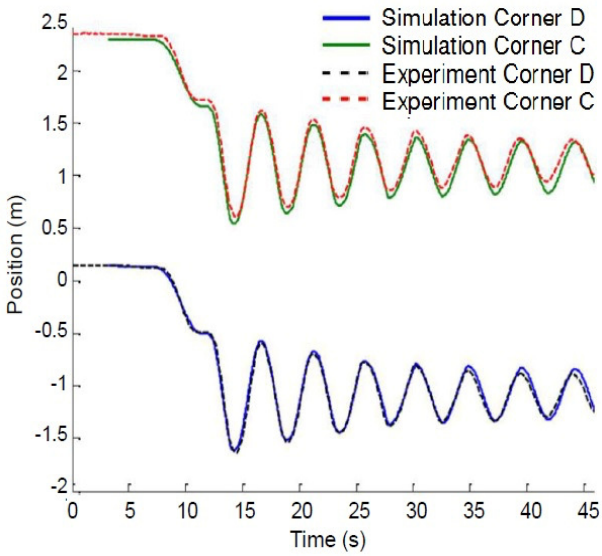

Figure 8: Horizontal Positions of Payload Bottom Corners (lift height of 5cm and initial offset of 1.2m).

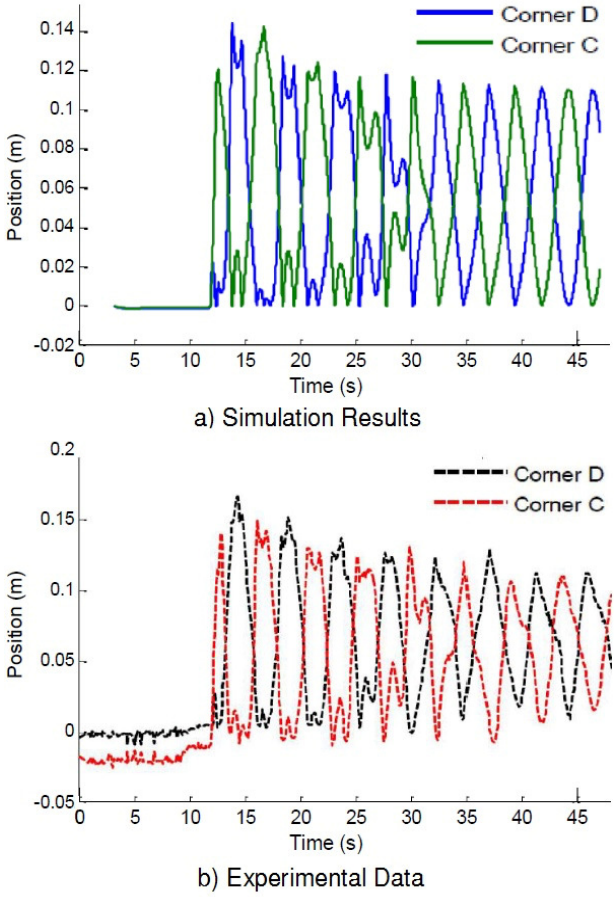

Figure 9: Vertical positions of payload bottom corners (5cm lift height, 1.2m initial offset).

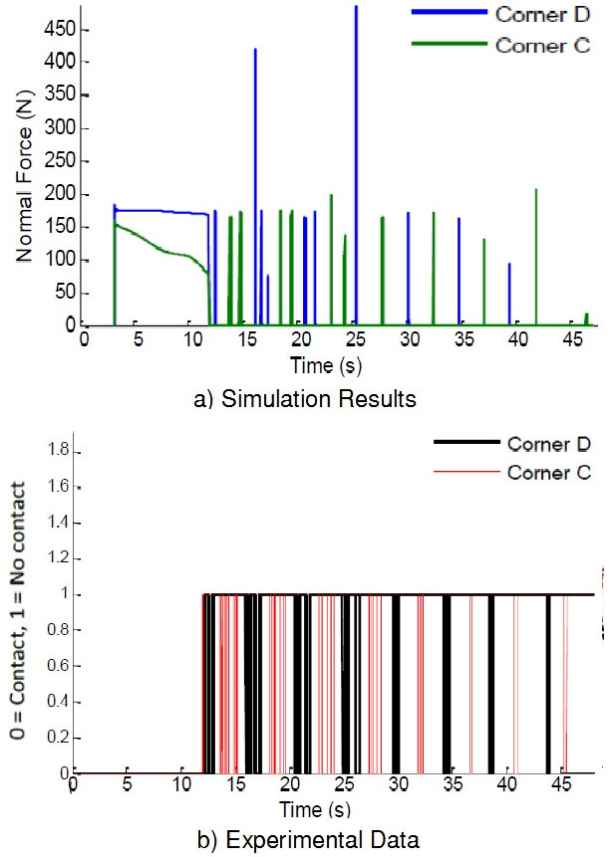

Figure 10: Contact instances of payload bottom corners with the ground (lift height of 5 mm and initial offset of 1.2 mm)

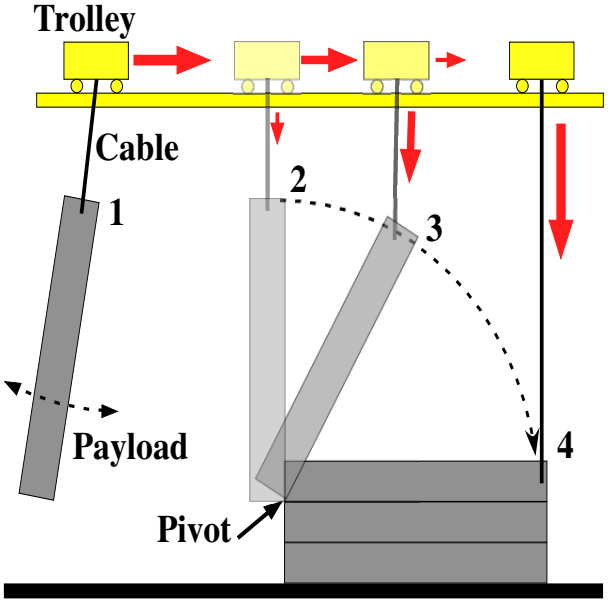

Figure 11: Steps in the Lay-Down Process.

4. PAYLOAD LAY-DOWN

The previous sections presented advancements in the modeling and understanding of payload lift-off dynamics. However, laying a payload down on the ground can also be a challenging task wherein the dynamic behavior is very important. This section will examine this problem by focusing on taking a long, vertically-suspended payload and laying it down flat on the ground.

Figure 11 illustrates a four-step lay-down maneuver of a long payload. It is assumed that the payload is attached to the hook and hoist cables and suspended in a vertical position. The crane operator transports the payload to the desired location in step 1. In step 2, the lay-down process begins, wherein the operator establishes a stationary pivot point on the lower end of the payload. During step 3, the operator simultaneously controls the trolley and lowers the hoist cables. The payload then rotates about the pivot, following a quarter circular arc from vertical to horizontal orientation. The lay-down maneuver is complete in step 4, where the payload is lying in a horizontal position.

Several potential problems can occur during the lay-down maneuver (steps 2-4 in Figure 11):

1. If the simultaneous movements of the trolley and lowering of the hoist cable are not properly coordinated then the payload pivot may slip and mvoe suddenly in unintended and unpredictable ways. This can potentially cause damage, lengthy down-times, and injure people. Due to the level of skill required in making these coordinated movements, highly experienced operators are usually employed.

2. “Side-pull” may occur during steps 2-4. This is when the hoist cable is at a steep angle relative to the hoist drum. Some typical problems associated with side pull include:

i. The cables may come out of the grooves on the hoist drum and rub against the remaining cables or drum, resulting in damaged cables.

ii. Side pull may cause unintended stress on certain crane components.

iii. Dangerous and unpredictable payload sliding and swinging.

The goal of the work presented in this section is to study the dynamics of lay-down maneuvers. Then, obtain motion-control solutions that aid operators to avoid the problems listed above. As the process of formulating lay-down dynamic models is similar to that of payload lift-up, similar analysis tools can be used. Coulomb friction is used to prescribe limit conditions pertaining to the payload pivot.

There is very little past work concerning the lay-down of long payloads. The closest work was by Hermann et al., who analyzed the dynamics of longitudinal pressure vessels and mobile cranes [21]. The focus of their paper, however, was on the erection of these pressure vessels, rather than the lay-down process. Traditionally, two or more mobile cranes are employed in such operations. Erection is difficult due to the complicated maneuvering and high levels of coordination between the cranes. Forces and motions during the process were modeled, which helped the design of an innovative rigging solution that could erect the long payload using only one crane.

One direct application of this work is in the lay-down of 30' (9.1m) aluminum ingots. The ingots are lifted vertically from smelting pits, and then transported to a storage area by a crane. The crane stores the ingots by stacking them horizontally using a lay-down procedure similar to that shown Figure 11. However, one of the main problems with this procedure is that operators can unintentionally put the crane in side-pull situations, where the hoist cable angle is too large. This can be a costly problem due to the frequent down-times that are required to repair the rubbing hoist cables and other crane components.

5. LAY-DOWN DYNAMICS

Figure 12 illustrates the dynamic model of the lay-down process and Figure 13 is the payload's free body diagram. The following describes the model and its assumptions:

1. Establishing the pivot, O, is not considered here. This is a highly-skilled task that is more suitable for manual operation. This is because establishing the pivot involves collisions, sliding, and stiction between surfaces. An automated solution would be impractical, as it would require many expensive sensors or extensive hardware modifications. Therefore, this research considers steps 2-4 in Figure 11

2. The payload has a width (into/out of the page) such that it has sufficient stability in the out of plane direction. Therefore, out of plane movements (e.g. buckling or trolley motions in that direction) are not considered. The payload length is also much greater than its thickness.

3. The pivot point, O, is the origin of the Cartesian coordinate reference frame. The frame axes unit vectors are i and j, as indicated in Figure 12.

4. The payload is modeled as a uniform slender beam of length L, pinned on the lower end at the pivot (assuming the pivot never moves), O. The payload angle from vertical is ϕ.

5. The higher end of the payload, P, is attached to a hoist cable of variable length, l. The angle of the cable relative to vertical is θ.

6. The other end of the hoist cable is attached to the trolley, which is assumed to be a movable point. It is located at a constant height, H, above the ground. The trolley motor controls the horizontal position, x.

7. The cable is modeled as massless and inextensible, because it is assumed that the payload mass is much larger than that of the cable. Additionally, the cable must always be in tension. The hoist motor controls the length of the cable, l.

8. The freebody diagram in Figure 13 shows four forces acting on the payload: cable tension, T; gravity, mg, acting at the mass center, G; and the reaction forces at O, F_i, and F_j.

9. The system has two degrees of freedom. However, there are four generalized coordinates of interest: ϕ, θ, x, and l. Specifying any two coordinates completely determines the configuration of the entire system.

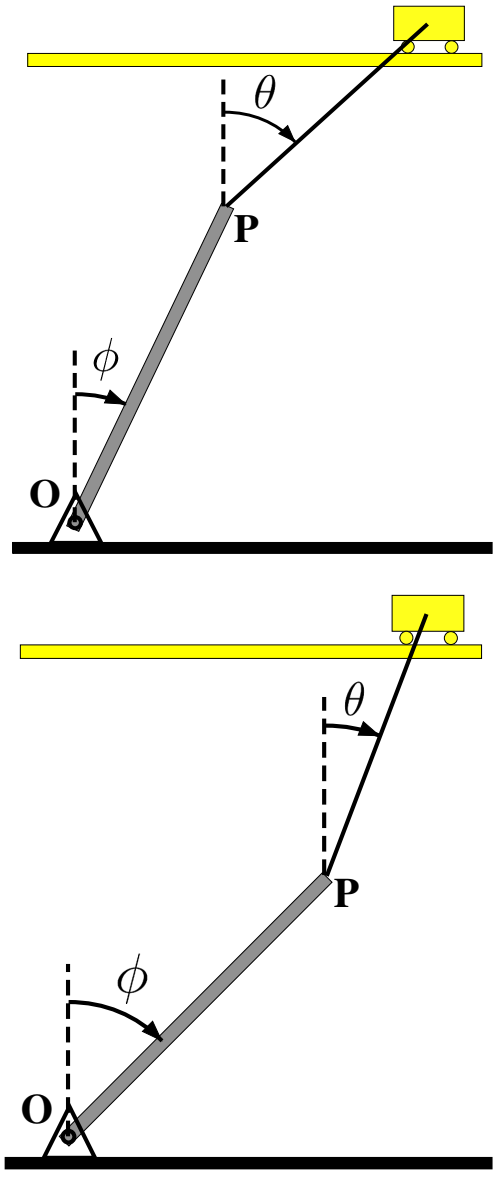

Figure 14: Unstable and Stable Configurations.

5.1 Range of Motions and Coordinate Relationships

The range of payload angles, ϕ, that are considered in this investigation is from 5° (nearly vertical position, after the operator has manually established the pivot) to 90° (horizontal position). The range of hoist cable angles, θ, that are considered is: $-90^{o}<\theta<\phi$.

The configuration specified by the lower bound on θ indicates that x would be negative infinity, which is physically impossible. The hoist cable angle upper bound is ϕ, because as the top of Figure 14 shows, a configuration with θ>ϕ is physically unstable. In these cases, the payload rotates under gravity to a more stable configuration, such that θ<ϕ, as shown in the bottom of Figure 14. Note that the position of the trolley, *x*, and the cable length, *l*, is the same in both configurations.

The following are positional constraints in the *i* and *j* directions that give the relationship between all four coordinates of interest: ϕ, θ, *x*, and *l*.

$$\begin{aligned} &L\cos\phi - l\cos\theta - H = 0 \\ &L\sin\phi - l\sin\theta - x = 0 \end{aligned} \tag{8}$$

5.2 Equations of Motion

The derivation of the dynamic equations of motion for the payload begins with the position vector from the pivot, O, to the payload mass center, G:

$$\vec{r}_{G/O} = \frac{L}{2}\left(\sin\phi\vec{i} + \cos\phi\vec{j}\right) \tag{9}$$

The acceleration of G is found by differentiating with respect to time:

$$\begin{aligned} &\vec{a}_G = -\ddot{\phi}\vec{k}\times\vec{r}_{G/O} - \dot{\phi}\vec{k}\times\left(-\dot{\phi}\vec{k}\times\vec{r}_{G/O}\right) = \\ &= \frac{L}{2}\left(\left(\ddot{\phi}\cos\phi - \dot{\phi}^2\sin\phi\right)\vec{i} + \left(-\ddot{\phi}\sin\phi - \dot{\phi}^2\cos\phi\right)\vec{j}\right) \end{aligned} \tag{10}$$

The equations of motion can be derived in terms of the two angles. First, the counter clockwise sum of moments about point O is (note that ϕ is defined to be positive in the clockwise direction):

$$\begin{aligned} &\sum M_O = -I\ddot{\phi} \\ &\Rightarrow TL\left(\cos\theta\sin\phi - \sin\theta\cos\phi\right) - \frac{1}{2}mgL\sin\phi = -I\ddot{\phi} \end{aligned} \tag{11}$$

where $I = \frac{1}{3}mL^2$ is the payload moment of inertia about O. Next, the sum of forces in the *i* direction is:

$$\begin{aligned} &\sum F\cdot\vec{i} = m\vec{a}_G\cdot\vec{i} \\ &\Rightarrow F_i + T\sin\theta = \frac{1}{2}mL\left(\ddot{\phi}\cos\phi - \dot{\phi}^2\sin\phi\right) \end{aligned} \tag{12}$$

And the sum of forces in the *j* direction is:

$$\begin{aligned} &\sum F\cdot\vec{j} = m\vec{a}_G\cdot\vec{j} \\ &\Rightarrow F_j + T\cos\theta - mg = \frac{1}{2}mL\left(-\ddot{\phi}\sin\phi - \dot{\phi}^2\cos\phi\right) \end{aligned} \tag{13}$$

5.3 Successful Lay-Down Conditions: Force Constraints

The primary condition for a successful lay-down maneuver, i.e. if the motion is stable in the dynamic sense, is that the pivot must not slip:

$$\left|\frac{F_i}{F_j}\right| \le \mu_{static} \tag{14}$$

where μ_{static} is the dry static coefficient of friction between the payload and the ground. Additionally, the payload must always maintain contact with the surface at the pivot:

$$F_j \ge 0 \tag{15}$$

and the cable must always be in tension:

$$T \ge 0 \tag{16}$$

Collectively, the above conditions are known as force constraints.

5.4 Allowable Static Configurations

To determine how to best lay down the payload, it is important to know bounds at which the system configuration becomes unstable. The first step in this investigation is to consider only the static case. That is, accelerations and velocities are set to zero such that the equations of motion are reduced to equations that balance forces and moments in static equilibrium:

$$\begin{aligned} &TL\left(\cos\theta\sin\phi - \sin\theta\cos\theta\right) - \frac{1}{2}mgL\sin\phi = 0 \\ &F_i + T\sin\theta = 0 \\ &F_j + \cos\theta - mg = 0 \end{aligned} \tag{17}$$

The above equations can be rearranged to explicitly show T, F_i, and F_j:

$$\begin{aligned} &T = \frac{mg\sin\theta}{2\sin\left(\phi-\theta\right)} \\ &F_i = -\frac{mg\sin\theta\sin\phi}{2\sin\left(\phi-\theta\right)} \\ &F_j = \frac{mg\left(\sin\phi\cos\theta - 2\cos\phi\sin\theta\right)}{2\sin\left(\phi-\theta\right)} \end{aligned} \tag{18}$$

Then, for each angle in the range of payload and hoist cable angles being considered, it can be determined whether the configuration is statically allowable. The range of statically stable and allowable configurations can then be determined.

5.4.1 Constraint on Cable Tension

By inspection, the tension is always positive, because $\sin\phi > 0$ for the range of ϕ considered; and $\sin(\phi-\theta) > 0$ because $\phi > \theta$ at all times. Therefore, the constraint on the cable always being in tension is always satisfied.

5.4.2 Constraint on Pivot Contact

The equation for F_j is used to determine whether the constraint on pivot contact with the surface is satisfied.

By inspection, $\sin\phi\cos\theta - 2\cos\phi\sin\theta \geq 0$ needs to be true in order to satisfy this constraint. Therefore, the condition on θ for pivot contact is:

$$\theta \leq \theta_c = \arctan\left(\frac{1}{2}\tan\phi\right) \tag{19}$$

5.4.3 Constraint on Pivot Slip

To determine the conditions on pivot slip, F_i is divided by F_j to yield:

$$\left|\frac{F_i}{F_j}\right| = \left|\frac{-\sin\phi\sin\theta}{\sin\phi\cos\theta - 2\cos\phi\sin\theta}\right| \tag{20}$$

This is then evaluated with the constraint on pivot slip to determine the range of hoist cable angles where the pivot does not slip. Defining:

$$\begin{aligned}\theta_{\mu 1} &= -\arctan\frac{\mu_{static}\sin\phi}{\sin\phi - 2\mu_{static}\cos\phi}, -\frac{\pi}{2} < \theta_{\mu 1} < \frac{\pi}{2}\\ \theta_{\mu 2} &= \arctan\frac{\mu_{static}\sin\phi}{\sin\phi + 2\mu_{static}\cos\phi}, -\frac{\pi}{2} < \theta_{\mu 2} < \frac{\pi}{2}\end{aligned} \tag{21}$$

the conditional cases on θ such that the pivot does not slip are:

$$\begin{aligned}&\theta_{\mu 1} < \theta < \theta_{\mu 2}, && \text{if } \theta_{\mu 1} < \theta_{\mu 2}\\ &\theta \geq \theta_{\mu 1} \text{ OR } \theta \leq \theta_{\mu 2} && \text{if } \theta_{\mu 1} > \theta_{\mu 2}\end{aligned} \tag{22}$$

5.5 Algorithm for Finding the Range of Allowable Static Configurations

The allowable static configurations are found by evaluating whether the constraints are satisfied by iterating though the entire range of angles:

for ϕin the range 5^o<ϕ< 90^o
forθ in the range -90^o<θ<ϕ
if (19) **AND** (22) are satisfied **then**
The configuration is statically allowable
else
The configuration is not statically allowable
end if
end for
end for

One insight to be gained from analyzing the constraints is that in the static case, the inequalities that describe the allowable configurations are only dependent on ϕ and μ_{static}. Therefore, these constraints are applicable to all payloads regardless of size, L, and mass, μ.

5.6 Allowable Static Configurations Example

An example with the crane and payload parameters in Table 2 is used to illustrate the process of finding allowable static configurations. These parameters reflect a typical aluminum ingot lay-down application.

Figure 15a) shows the forces as a function of θ for ϕ=10^o. This is the case when the payload is close to a vertical position near the start of lay-down. As the cable angle approaches 0^o from -90^o, the cable tension increases, but the vertical pivot force, F_j, decreases. This makes sense, because as the cable angle becomes more vertical, an increasing portion of the payload's weight is supported by the cable tension, rather than the contact at the pivot. The critical angle at which the pivot begins to lose contact with the surface, i.e. when F_j = 0, is indicated on the figure as θ_c. In this case, the payload will lose pivot contact when θ increases beyond a few degrees above 0. Also, note that pivot horizontal forces, F_i, are relatively small until θ approaches the value of ϕ.

Table 2: Aluminum Ingot Lay-Down Example: Crane and Payload Parameters.

Parameter	Value
m	8400 kg
L	10 m
H	12 m
μ_{static}	0.6 (Aluminum and mild steel, dry)

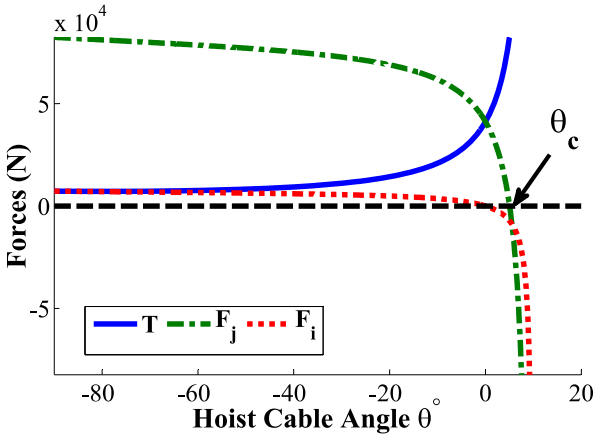

a)

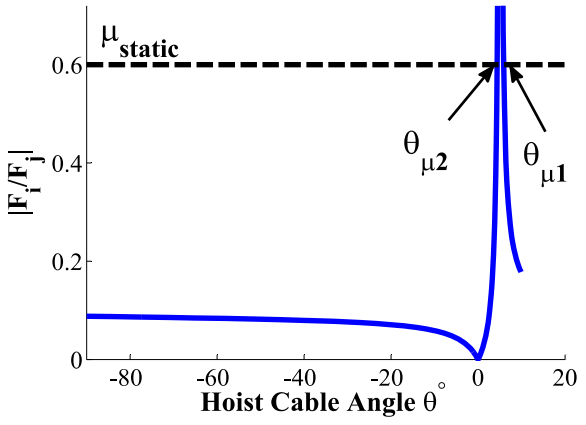

b)

Figure 15: Example Static Case, ϕ = 10^o.

Figure 15b) shows the ratio of horizontal to vertical pivot force for the same range of configurations. In this case, $\theta_{\mu 1} > \theta_{\mu 2}$. The figure also shows that the force ratio will exceed μ_{static} (i.e. the pivot will slip) in a narrow range between $\theta_{\mu 1}$ and $\theta_{\mu 2}$. However, note that this may be inconsequential, depending on the location of θ_c in Figure 15b). For example, if $\theta_c < \theta_{\mu 2}$, then the pivot would have already lost contact before it can slip.

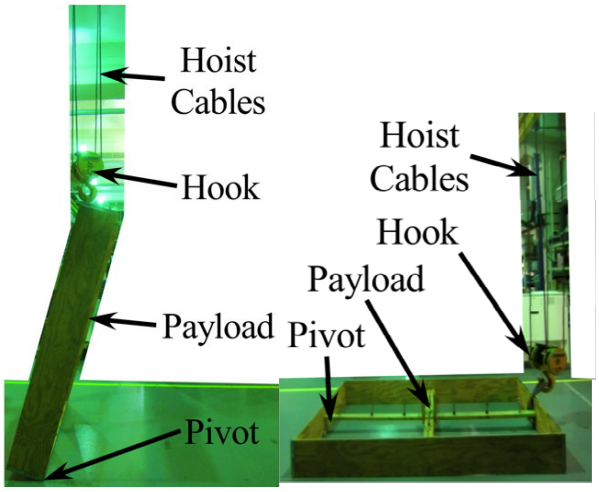

b)

Figure 16: Wooden Box Payload For Lay-Down Experiments.

5.7 Example Lay-Down Using a Bridge Crane

The methods presented above were implemented on the 10-ton bridge crane. The payload was a long wooden box. Figure 16a) is a picture that shows the experimental setup, when the payload is positioned close to upright at the start of the lay-down maneuver. Figure 16b) shows the payload in the finish position. Note there is a hook that connects the hoist cables to the payload. However, for the purpose of this demonstration, the effects of the hook can be neglected.

Figure 17 shows the static and dynamic boundaries of allowable configurations in the payload angle, ϕ–θ space. (The dynamic boundaries are formed by using additional motor constraints that limit the velocities and accelerations of the trolley and hoist motors.) Two features are worth noting: 1) compared to the aluminum ingot example, the range of allowable configurations begins to narrow starting at a lower value when ϕ is approximately 35°; and 2) the dynamic boundaries are very similar to the static boundaries. Therefore, the static boundaries can be used to determine the lay-down trajectory.

Figure 18 shows an example trajectory superimposed on the surface of allowable configurations plotted in the ϕ-*x*-*l* space. The trajectory starts around payload angle ϕ =5°, and finishes at ϕ =90 °. Each point on the trajectory specifies the trolley position, *x*, and hoist cable length, *l*.

A few points were selected from the trajectory. Then, trolley and hoist motor velocity command profiles were generated to drive the crane to the selected configurations. The positions of the lower pivot end of the wooden box (point O in the lay-down schematic diagram of Figure 12), and the upper end where it is attached to the hook (point P in Figure 12) were tracked using radio-frequency location tags.

Figure 19 shows the measured tag positions during the execution of the lay-down velocity commands. The upper end follows approximately a quarter circular arc as the payload is laid down from a near-upright position to a horizontal position. Figure 20 shows the trajectory of the configuration during the lay-down maneuver. The trajectory remained well inside the static boundaries throughout the move.

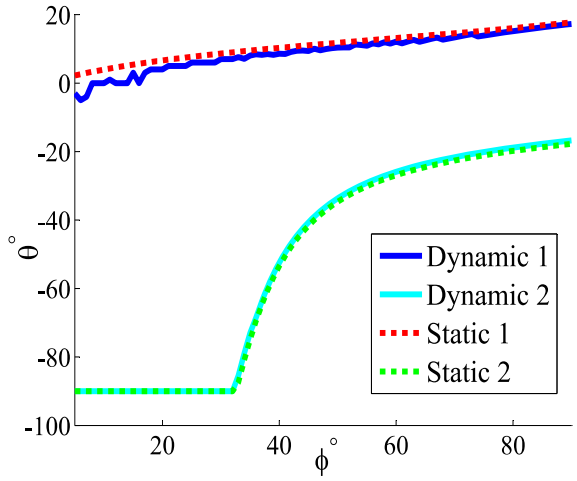

Figure 17: Wooden Box Allowable Configurations in Terms of Payload Angle, ϕ, vs. Cable Angle, θ.

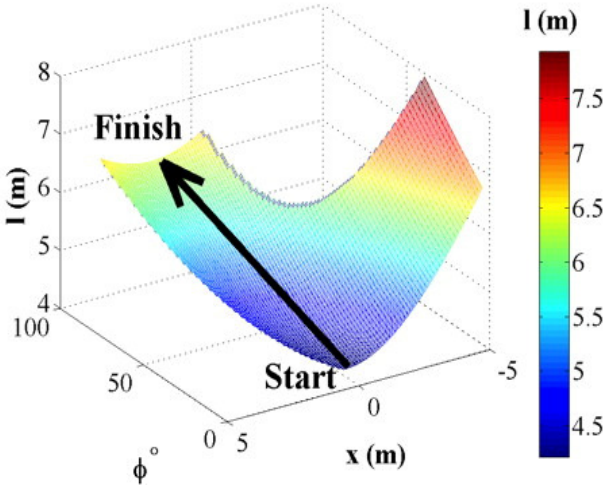

Figure 18: Example Trajectory in Terms of Payload Angle, ϕ, vs. Trolley Position, *x*, vs. Hoist Cable Length, *l*.

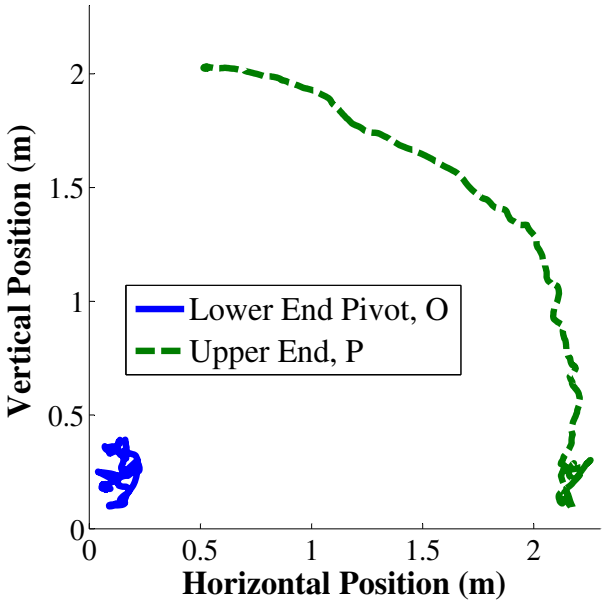

Figure 19: Wooden Box Lay-Down Experimental Trajectories - Positions of Lower and Upper Payload Ends.

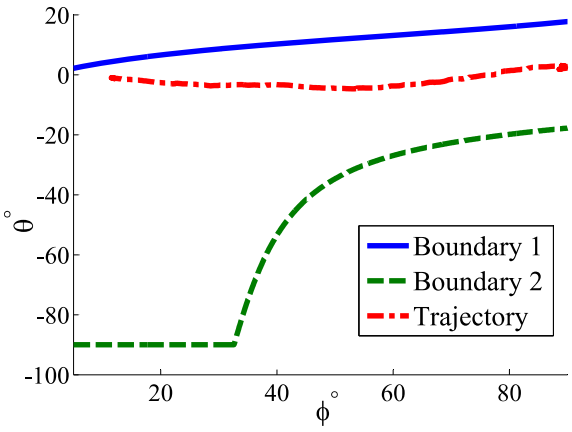

Figure 20: Wooden Box Lay-Down Experimental Trajectories - Payload Angle, ϕ, vs. Cable Angle, θ.

6. CONCLUSIONS

A model was developed to predict the dynamic response of cranes performing off-centered lifts. It was demonstrated that the model was able to accurately capture dynamics of a variety of contact modes that exist between the payload and ground during an off-centered lift, such as sliding, stiction, impact, and swinging. More importantly, it accomplishes this without having to handle contact modes separately and simulating transition laws between dynamic modes. This approach allows for the model to naturally extend from two-dimensional planar motions to three-dimensional off-centered crane lifts. The dynamics of lay-down operations were also examined. Motion-profiles that achieve stable lay-down results were developed. Experimental results from a 10-ton bridge crane were used to verify the accuracy of both the lift-off and lay-down dynamics.

ACKNOWLEDGEMENTS

We would like to thank National Instrument for donating the myRio controller that was used in the experimental setup to capture payload/ground interactions.

REFERENCES

[1] R. L. Neitzel, N. S. Seixas, and K. K. Ren, "Review of crane safety in the construction industry," *Applied Occupational and Environmental Hygiene*, vol. 16, No. 12, pp. 1106-1117, 2001.

[2] R. G. Garby, *IPT's Crane and Rigging Handbook*: IPT Publishing and Training Ltd2005.

[3] E. M. Abdel-Rahman, A. H. Nayfeh, and Z. N. Masoud, "Dynamics and Control of Cranes: A Review," *Journal of Vibration and Control*, vol. 9, No. 7, pp. 863-908, 2003.

[4] W. Singhose, L. Porter, M. Kenison, and E. Kriikku, "Effects of Hoisting on the Input Shaping Control of Gantry Cranes," *IFAC Control Engineering Practice*, vol. 8, No. 10, pp. 1159-1165, 2000.

[5] J. Stergiopoulos and A. Tzes, "An Adaptive Input Shaping Technique for the Suppression of Payload Swing in Three-Dimensional Overhead Cranes with Hoisting Mechanism," IEEE Int. Conference on Emerging Technologies and Factory Automation, Patras, Greece, pp. 565-68, 2007.

[6] D. Kim and W. Singhose, "Reduction of Double Pendulum Crane Oscillations," Int. Conf. on Motion and Vibration Control, Daejeon, Korea, 2006.

[7] M. A. Ahmad, R. M. T. R. Ismail, M. S. Ramli, A. N. K. Nasir, N. M. Abd Ghani, and N. H. Noordin, "Comparison of Input Shaping Techniques for Sway Suppression in a Double-Pendulum-Type Overhead Crane," Computer Modeling and Simulation, 2009. EMS '09. Third UKSim European Symposium on, pp. 321-326, 2009.

[8] D. Kim and W. Singhose, "Performance Studies of Human Operators Driving Double-Pendulum Bridge Cranes," *IFAC Control Engineering Practice*, vol. 18, No. June, pp. 567-576, 2010.

[9] R. Manning, J. Clement, D. Kim, and W. Singhose, "Dynamics and Control of Bridge Cranes Transporting Distributed-Mass Payloads," *ASME J. Dynamic Systems, Measurement, and Control*, vol. 132, No. Jan., pp. 014505-3, 2010.

[10] D. A. Barrett and T. M. Hrudey, "An Investigation of Hoist-induced Dynamic Loads on Bridge Crane Structures," *Canadian Journal of Civil Engineering*, vol. 23, No. 4, pp. 92-939, 1996.

[11] M. T. Mason, *Mechanics of Robotic Manipulation*: The MIT Press2001.

[12] K. Sorensen and W. Singhose, "Crane Motion Control,"

[13] Camotion.com/SOLUTIONS/CRANECONTROL/tabid/359/Default.aspx, accessed Nov., 2013.

[14] A. Garcia, et al., "Three-Dimensional Modeling and Experimental Verification of Off-Centered Crane Lifts," Dynamic Systems and Control Conference, Columbus, OH, 2015.

[15] K. C.-C. Peng, "Methods for Improving Crane Performance and Ease of use," Georgia Institute of Technology, 2013.

[16] V. V. Geffen, "A Study of Friction Models and Friction Compensation," Technische Universiteit Eindhoven December 2009.

[17] C. Glocker and F. Pfeiffer, "An LCP-Approach for Multi-body Systems with Planar Friction," Proc. Contact Mechanics Int. Sym., pp. 13-30, 1992.

[18] G. Gilardi and I. Sharf, "Literature Survey of Contact Dynamics Modelling," *Mechanisms and Machine Theory*, vol. 37, No. 10, pp. 1213-1239, 2002.

[19] A. A. Ferri, "Modeling and Analysis of Nonlinear Sleeve Joints of Large Space Structures," *Journal of Spacecraft and Rockets*, vol. 25, No. 5, pp. 354-360, 1988.

[20] J. Kyle and M. Costello, "Comparison of Measured and Simulated Motion of a Scaled Dragline Excavation System," *Elsevier Mathematical and*

Computer Modelling, vol. 44, No. 9-10, pp. 816-833, 2006.

[21] U. H. Hermann, S. Hasan, M. Al-Hussein, and A. Bouferguene, "Innovative system for off-the-ground rotation of long objects using mobile cranes," *Journal of Construction Engineering and Management*, vol. 137, No. 7, pp. 478-485, 2011.

МОДЕЛОВАЊЕ И УПРАВЉАЊЕ ДИЗАЛИЧНИМ ОПЕРАЦИЈАМА ПОДИЗАЊА И СПУШТАЊА КОРИСНОГ ТЕРЕТА

В. Сингхос, К. Пенг, А. Гарсија, А. Фери

Када дизалица подиже терет са земље може доћи до његовог неочекиваног љуљања у страну. Ово се дешава када терет није директно испод витла у вертикалном правцу. Како је велико растојање између витла и терета, руковаоци дизалицом не могу да знају да ли је уже, пре почетка операције дизања терета, потпуно у вертикалном положају. При подизању терета по правилу долази до његовог хоризонталног кретања у одређеном опсегу. Ако се врши дизање терета које није у вертикали са витлом долази до његовог значајног хоризонталног кретања, настаје опасност по руковаоце дизалицом, терет и околину. У раду се приказују динамички модели подизања терета вертикално померених у односу на витло као и експериментална верификација теоријских претпоставки. Инверзни проблем спуштања великог терета на земљу може такође да представља изазов. На пример, када се спушта дугачак терет у хоризонтални положај на равној површини, полазећи од приближне вертикалне оријентације у ваздуху, терет може неочекивано да склизне у страну. Рад приказује решења за управљање кретањем која могу помоћи руковаоцима дизалицом у извођењу операције спуштања терета, која је пуна изазова.